Phases and transitions in the spin-1 Bose-Hubbard model: Systematics of a mean-field theory

Ramesh V. Pai*
Department of Physics, Goa University, Taleigao Plateau, Goa 403 206, India

K. Sheshadri†
686, BEL Layout, 3rd Block, Vidyaranyapura, Bangalore 560 097, India

Rahul Pandit‡
Centre for Condensed Matter Theory, Department of Physics, Indian Institute of Sciences, Bangalore 560 012, India
(Received 15 May 2007; revised manuscript received 27 November 2007; published 8 January 2008)

We generalize the mean-field theory for the spinless Bose-Hubbard model to account for the different types of superfluid phases that can arise in the spin-1 case. In particular, our mean-field theory can distinguish polar and ferromagnetic superfluids, Mott insulator, that arise at integer fillings at zero temperature, and normal Bose liquids into which the Mott insulators evolve at finite temperatures. We find, in contrast to the spinless case, that several of the superfluid-Mott insulator transitions are of first order at finite temperatures. Our systematic study yields rich phase diagrams that include first-order and second-order transitions and a variety of tricritical points. We discuss the possibility of realizing such phase diagrams in experimental systems.

DOI: 10.1103/PhysRevB.77.014503 PACS number(s): 67.10.Fj, 03.75.Mn, 05.30.Jp, 73.43.Nq

I. INTRODUCTION

Experimental investigations of ultracold atoms in optical lattices have opened up a new realm in the study of quantum phase transitions.[1,2] The superfluid (SF) to Mott-insulator (MI) transition has been observed in spin-polarized ^{87}Rb atoms trapped in a three-dimensional, optical-lattice potential,[3] by changing the strength of the on-site potential, as predicted theoretically by studies of the spinless Bose-Hubbard model.[4–6] Furthermore, technical advances in the trapping of atoms by purely optical means[7] have enhanced the interest in the study of quantum magnetism in confined dilute atomic gases. Alkali atoms with nuclear spin $I=3/2$, such as ^{23}Na, ^{39}K, and ^{87}Rb, have hyperfine spin $F=1$. In conventional *magnetic traps*, these spins are frozen, so the atoms can be treated as spinless bosons; by contrast, in *purely optical traps*, these spins are free, so the Bose condensates, which form at low temperatures, can have a spinor nature[8–10] and the SF-MI transition can be modified.[1–13] In the spinless case, the SF-MI transition, which occur, at fixed boson density, when the number of bosons per site is an integer, is controlled by the interaction U_0 between bosons at the same site. As U_0 increases beyond a critical value U_{0C}, the SF phase undergoes a continuous transition to a MI phase; this is reflected in the development of a gap at the transition. When the spin is nonzero, such a gap also develops at the SF-MI transition, but the properties of the phases and the nature of these transitions are modified by the spin degrees of freedom.

Theoretical work on this problem has dealt primarily with the properties of spinor condensates by using a continuum, effective, low-energy Hamiltonian. Such a Hamiltonian suffices if one is interested in the natures of the superfluid phases, which can be polar or ferromagnetic, and in their excitations, which include vector or quadrupolar spin waves and topological defects.[8–10] However, if we want to study the SF-MI transitions, we must use a lattice model such as the spin-1 Bose-Hubbard model. Some groups[11–13] have initiated such an investigation by obtaining the zero-temperature phase diagram of this model in a mean-field approximation. The topology of this phase diagram for the spin-1 Bose-Hubbard model is similar to that of its spinless counterpart, but, in the spin-1 model, the superfluid phases can be either polar or ferromagnetic depending on whether the spin-dependent interaction favors or disfavors the formation of singlets. In the former case, the SF-MI phase transition is *continuous* if the density of bosons per site ρ is an odd number, but is of *first order* if ρ is an even number.

We have two main goals in this paper: The first is to give a global view of the zero-temperature, mean-field-theory phase diagram of the spin-1 Bose-Hubbard model, emphasizing issues of first-order coexistence that have not been highlighted so far. The second is to generalize this mean-field theory to finite temperatures $T>0$ and, thus, obtain the finite-temperature, mean-field-theory phase diagram for this model.

The spin-1 Bose-Hubbard model is defined by the Hamiltonian

$$\mathcal{H} = -t \sum_{\langle i,j\rangle,\sigma} (a^{\dagger}_{i,\sigma} a_{j,\sigma} + \text{H.c.}) + \frac{U_0}{2} \sum_i \hat{n}_i(\hat{n}_i - 1) + \frac{U_2}{2} \sum_i (\vec{F}_i^2 - 2\hat{n}_i) - \sum_i \mu_i \hat{n}_i, \quad (1)$$

where the first term is the kinetic energy associated with the hopping of bosons between nearest-neighbor pairs of sites $\langle i,j\rangle$ with amplitude t, $a^{\dagger}_{i,\sigma}$ ($a_{i,\sigma}$) is the boson creation (annihilation) operator at site i with spin component σ (that can assume the values 1, 0, and −1), $\hat{n_{i\sigma}} \equiv a^{\dagger}_{i,\sigma} a_{i,\sigma}$, $\hat{n_i} \equiv \Sigma_\sigma \hat{n_{i,\sigma}}$, and $\vec{F}_i = \Sigma_{\sigma,\sigma'} a^{\dagger}_{i,\sigma} \vec{F}_{\sigma,\sigma'} a_{i,\sigma'}$ are, respectively, the total boson number and spin on site i, and $\vec{F}_{\sigma,\sigma'}$ are the standard spin-1 matrices; U_0 is the on-site Hubbard repulsion and U_2 is the energy for nonzero spin configurations on a site. The origin of such a spin-dependent term lies in the difference between

the scattering lengths a_0 and a_2, for $S=0$ and $S=2$ channels,[14] respectively; in terms of these lengths, $U_0=4\pi\hbar^2(a_0+2a_2)/3M$ and $U_2=4\pi\hbar^2(a_2-a_0)/3M$, where M is the mass of the atom.[8] For ^{23}Na, $a_2=54.7a_B$ and $a_0=49.4a_B$, where a_B is the Bohr radius, so $U_2>0$, whereas for ^{87}Rb, $a_2=(107\pm4)a_B$ and $a_0=(110\pm4)a_B$, so U_2 can be negative. The parabolic trapping potential with strength V_T is represented by the site-dependent chemical potential $\mu_i=\mu-V_T|R_i|^2$, where R_i is the distance of site i from the center of the trap and μ is a uniform chemical potential that controls the mean density of the bosons. In this study, we neglect the trap potential (i.e., we set $V_T=0$) and focus on the effects of the spin degrees of freedom. However, the mean-field theory described below can be generalized to discuss the case with $V_T>0$.

The zero-temperature phase diagram of model (1) has been obtained in the mean-field approximation by some groups.[11–13] We have extended these studies significantly. Before presenting the details of our work, we give a qualitative overview of our results.

Consider first the case $U_2=0$: We might expect the spin-1 and spinless Bose-Hubbard models to have the same phase diagram in this case since the ground-state energy does not depend on the spin. This is superficially true at $T=0$ in so far as the SF-MI phase boundaries for both these models overlap. However, as we will show, the SF phase is highly degenerate in the spin-1 case and, for $T>0$, the SF-MI transition becomes of first order and, eventually, is continuous again. Thus, the finite-temperature phase diagram has a rich topology, with first-order boundaries evolving into continuous ones at tricritical points.

If $U_2\neq0$, the on-site interaction between the bosons becomes spin dependent. It turns out that we must distinguish between the cases $U_2<0$ and $U_2>0$. The former has a phase diagram that is very similar to that for $U_2=0$; the major qualitative difference arises in the nature of the SF phase that is now a ferromagnetic superfluid.

There are many differences between the phase diagrams of the spin-1 model with $U_2=0$ and $U_2>0$. If $U_2>0$, the SF phase is a polar superfluid. Furthermore, even at $T=0$, the SF-MI transitions are different for odd and even densities. For odd densities, the $T=0$ SF-MI transition is continuous as for $U_2=0$; however, for even densities, this SF-MI transition turns out to be of first order because of the formation of singlets that also stabilize the MI phase considerably.

At finite temperatures, the MI phases evolve without a singularity into a normal Bose liquid (NBL). These are really not distinct phases, but, as we will show, the compressibility κ can be used effectively to delineate the crossover between MI and NBL regions.

To present our results in detail, we must introduce our mean-field theory. We do this in Sec. II. Our results are given in Sec. III. We end with a discussion in Sec. IV.

II. MEAN-FIELD THEORY

Mean-field theory has been very successful in obtaining the phase diagram for the spinless Bose-Hubbard model.[5,6] There are three formulations of this mean-field theory: one uses a model with infinite-range interactions, another a Gutzwiller-type wave function, and a third,[5] which we follow, a decoupling approximation. The unique feature of this decoupling scheme is that, unlike conventional mean-field theories, it does not decouple the interaction term to obtain an effective one-particle problem but, instead, decouples the hopping term to obtain an effective one-site problem. This one-site problem is then solved self-consistently. We generalize the decoupling procedure to the spin-1 case as follows:[5] In the identity $a^\dagger_{i,\sigma}a_{j,\sigma}=(a^\dagger_{i,\sigma}-\langle a^\dagger_{i,\sigma}\rangle)(a_{j,\sigma}-\langle a_{j,\sigma}\rangle)+\langle a^\dagger_{i,\sigma}\rangle a_{j,\sigma}+a^\dagger_{i,\sigma}\langle a_{j,\sigma}\rangle-\langle a^\dagger_{i,\sigma}\rangle\langle a_{j,\sigma}\rangle$, where $\langle\mathcal{O}\rangle$ denotes the equilibrium value of an operator $\mathcal{O}$, we neglect the first term that is quadratic in deviations from the equilibrium value. Thus,

$$a^\dagger_{i,\sigma}a_{j,\sigma}\simeq\langle a^\dagger_{i,\sigma}\rangle a_{j,\sigma}+a^\dagger_{i,\sigma}\langle a_{j,\sigma}\rangle-\langle a^\dagger_{i,\sigma}\rangle\langle a_{j,\sigma}\rangle. \tag{2}$$

Since we expect superfluid phases, it is natural to introduce the superfluid order parameters

$$\psi_\sigma\equiv\langle a^\dagger_{i,\sigma}\rangle\equiv\langle a_{i,\sigma}\rangle \tag{3}$$

for $\sigma=1$, 0, and -1. We consider equilibrium states with uniform phases, so we choose these order parameters to be real. (For the case $V_T>0$, ψ_σ also depends on the site label i; see Sec. IV.) Given the decoupling approximation (2), the Hamiltonian (1) can be written as a sum over single-site, mean-field (MF) Hamiltonians:

$$\mathcal{H}=\sum_i\mathcal{H}_i^{MF}, \tag{4}$$

where

$$\mathcal{H}_i^{MF}=\frac{U_0}{2}\hat{n}_i(\hat{n}_i-1)+\frac{U_2}{2}(\vec{\hat{F}}_i^2-2\hat{n}_i)-\mu\hat{n}_i-\psi_\sigma(a^\dagger_{i,\sigma}+a_{i,\sigma})+\sum_\sigma|\psi_\sigma|^2. \tag{5}$$

We set the energy scale by choosing $zt=1$, where z is the number of nearest neighbors. At least one of the order parameters ψ_σ is nonzero in a superfluid phase. In order to calculate ψ_σ in our mean-field theory, we first obtain the matrix elements of the mean-field Hamiltonian $\mathcal{H}_i^{MF}$ in the on-site, occupation-number basis $\{|n_{i,-1},n_{i,0},n_{i,1}\rangle\}$ truncated at a finite value n_{max} of the total number of bosons per site $n_i=\Sigma_\sigma n_{i,\sigma}$. In most of our studies, we use $n_{max}=4$, for which the mean-field Hamiltonian is a 35×35 matrix.[15] We diagonalize this matrix to obtain its eigenvalues $\mathcal{E}_\alpha$ and eigenvectors $|\varphi_\alpha\rangle$:

$$\mathcal{H}_i^{MF}|\varphi_\alpha\rangle=\mathcal{E}_\alpha|\varphi_\alpha\rangle; \tag{6}$$

we suppress the site index i on these eigenvalues and eigenvectors since all the phases we consider are spatially uniform.

We now obtain the variational free energy

$$\mathcal{F}(\mu,U_0,U_2,T;\psi_\sigma)=-T\ln Z(\mu,U_0,U_2,T;\psi_\sigma), \tag{7}$$

where $Z(\mu,U_0,U_2,T;\psi_\sigma)$ is the partition function

$$Z(\mu, U_0, U_2, T; \psi_\sigma) = \sum_\alpha e^{-\mathcal{E}_\alpha/T}, \tag{8}$$

with the Boltzmann constant k_B chosen to be 1. The variational free energy $\mathcal{F}$ must be minimized with respect to the order parameters ψ_σ, i.e., we must solve the equations $\partial\mathcal{F}/\partial\psi_\sigma = 0$ for $\sigma = 1$, 0, and -1. These equations can be recast as self-consistency conditions for ψ_σ; solutions of these self-consistency conditions correspond to extrema of $\mathcal{F}$. In case there is more than one solution, we must pick the one that yields the global minimum of $\mathcal{F}$. (At a first-order phase boundary, $\mathcal{F}$ has two, equally deep, global minima.) The values of ψ_σ and $\mathcal{F}$ at the global minimum yield the equilibrium order parameters ψ_σ^{eq} and free energy $\mathcal{F}^{eq}$. In our mean-field theory, the superfluid density is

$$\rho_s = \sum_\sigma |\psi_\sigma^{eq}|^2. \tag{9}$$

The magnetic properties of the superfluid phases of this model are obtained from[8]

$$\langle \vec{F} \rangle = \frac{\sum_{\sigma,\sigma'} \psi_\sigma^{eq} \vec{F}_{\sigma,\sigma'} \psi_{\sigma'}^{eq}}{\sum_\sigma |\psi_\sigma^{eq}|^2}; \tag{10}$$

the explicit forms of the spin-1 matrices now yield

$$\langle \vec{F} \rangle = \sqrt{2}\frac{(\psi_1\psi_0 + \psi_{-1}\psi_0)}{\sum_\sigma |\psi_\sigma|^2}\hat{x} + \frac{(\psi_1^2 - \psi_{-1}^2)}{\sum_\sigma |\psi_\sigma|^2}\hat{z},$$

$$\langle \vec{F} \rangle^2 = 2\frac{(\psi_1\psi_0 + \psi_{-1}\psi_0)^2}{\left(\sum_\sigma |\psi_\sigma|^2\right)^2} + \frac{(\psi_1^2 - \psi_{-1}^2)^2}{\left(\sum_\sigma |\psi_\sigma|^2\right)^2}, \tag{11}$$

where $\hat{x}$ and $\hat{z}$ are unit vectors in spin space, and we suppress the superscript eq for notational convenience; all ψ_σ used here and henceforth are actually ψ_σ^{eq}. Superfluid states with $\langle \vec{F} \rangle = 0$ and $\langle \vec{F} \rangle^2 = 1$ are referred to as polar and ferromagnetic, respectively. The polar state has an order-parameter manifold $[U(1) \times S^2]/\mathbb{Z}_2$, where $U(1)$ denotes the phase angle θ, S^2 refers to the directions $\hat{\mathbf{n}}$ on the surface of a unit sphere [on which orientations are specified by the angles (α, β) of the spin quantization axis], and $\mathbb{Z}_2$ arises because of the symmetry of this state under the simultaneous transformations $\theta \to \theta + \pi$ and $\hat{\mathbf{n}} \to -\hat{\mathbf{n}}$. Thus, the superfluid order parameters can be written as

$$\begin{pmatrix} \psi_1 \\ \psi_0 \\ \psi_{-1} \end{pmatrix} = \sqrt{\rho_s} e^{\iota\theta} \begin{pmatrix} -\frac{1}{\sqrt{2}} e^{-\iota\alpha} \sin\beta \\ \cos\beta \\ \frac{1}{\sqrt{2}} e^{\iota\alpha} \sin\beta \end{pmatrix}. \tag{12}$$

Similarly, since the ferromagnetic superfluid state has an order-parameter manifold with the symmetry group $SO(3)$,

TABLE I. The superfluid density ρ_s, $\langle \vec{F} \rangle^2$, and the compressibility κ in the different phases of the spin-1 Bose-Hubbard model. The MI and NBL are really the same phase (see text).

Phases	ρ_s	$\langle \vec{F} \rangle^2$	κ
Polar superfluid (PSF)	>0	0	>0
Ferro superfluid (FSF)	>0	1	>0
Mott insulator (MI)	0		0
Normal bose liquid (NBL)	0		>0

$$\begin{pmatrix} \psi_1 \\ \psi_0 \\ \psi_{-1} \end{pmatrix} = \sqrt{\rho_s} e^{\iota(\theta-\tau)} \begin{pmatrix} e^{-\iota\alpha} \cos^2\frac{\beta}{2} \\ \sqrt{2}\cos\frac{\beta}{2}\sin\frac{\beta}{2} \\ e^{\iota\alpha}\sin^2\frac{\beta}{2} \end{pmatrix}, \tag{13}$$

where α, β, and τ are Euler angles.

We consider only spatially uniform superfluids in equilibrium, so it suffices to use real order parameters. Thus, for the polar superfluid, we have the following possibilities: (i) $\psi_1 = \psi_{-1} > 0$ and $\psi_0 = 0$ with $\theta = \alpha = \beta = \pi/2$ or $\theta = -\alpha = \beta = \pi/2$; and (ii) $\psi_1 = \psi_{-1} = 0$ and $\psi_0 > 0$ with $\beta = 0$ or π, $\theta = 0$ or π, and $0 \leqslant \alpha \leqslant 2\pi$. Similarly for the ferromagnetic superfluid $\psi_1 = \psi_{-1}$, $\beta = \pi/2$, $\alpha = 0$, $0 < \theta = \tau \leqslant 2\pi$, and $\psi_0 = \sqrt{2}\psi_1$.

The equilibrium density ρ and compressibility κ can be obtained from

$$\rho = -\frac{\partial \mathcal{F}^{eq}}{\partial \mu} = \frac{1}{Z}\sum_\alpha e^{-E_\alpha/T}\langle \phi_\alpha | \hat{n} | \phi_\alpha \rangle, \tag{14}$$

where E_α and $|\phi_\alpha\rangle$ are $\mathcal{E}_\alpha$ and $|\varphi_\alpha\rangle$ at the global minimum of $\mathcal{F}$ and

$$\kappa = \frac{\partial \rho}{\partial \mu}. \tag{15}$$

The three quantities ρ_s, $\langle \vec{F} \rangle^2$, and κ together determine the thermodynamic phase of model (1) for any point in the parameter space $\{\mu, U_0, U_2, T\}$ as given in Table I. Strictly speaking, there is no distinction between the MI and the NBL. The former exists at $T = 0$ and has $\kappa = 0$; it evolves without any singularity into the NBL at $T > 0$. At low T, the compressibility κ is exponentially small in the NBL so one can think of it as a MI phase. At high T, κ is substantially different from 0; it is best to think of this phase as a normal Bose liquid. It is convenient, therefore, to define a crossover boundary above which κ is substantial; we use the criterion $\kappa = \kappa_X$ (we use $\kappa_X = 0.01$, 0.002, or 0.03) to obtain the MI-NBL crossover boundary shown in some of our phase diagrams. We must remember, of course, that this is not a strict phase boundary and it depends on the value we choose for the crossover compressibility κ_X.

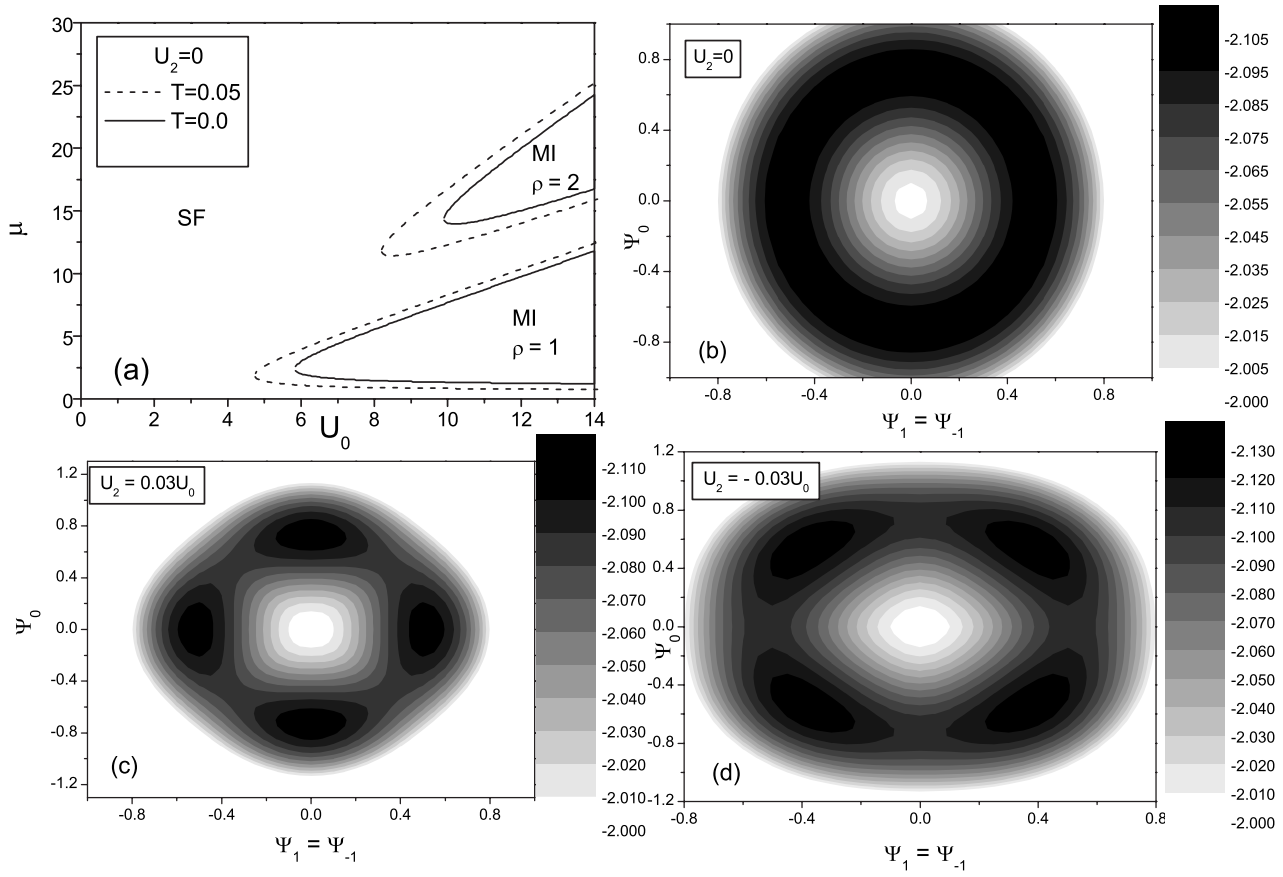

FIG. 1. (a) Phase diagrams in the (μ-U_0) plane for U_2=0: Solid lines indicate the T=0 continuous phase boundaries between SF and MI phases; these phase boundaries evolve into first-order boundaries at finite (but low) temperatures as shown by the representative dashed lines for T=0.05. At higher temperatures, these first-order boundaries become continuous again at lines of tricritical points. Pseudograyscale plots at T=0 of the variational ground-state energy $\mathcal{E}_0$ for (b) U_2=0, (c) U_2/U_0=0.03, and (d) U_2/U_0=−0.03, respectively; the four degenerate minima in (c) and (d) show that the SF phase is polar in the former and ferromagnetic in the latter. In (b), i.e., U_2=0, the SF phase is infinitely degenerate (see text).

III. RESULTS

We are now in a position to present the results of our mean-field theory. It is necessary to distinguish between three qualitatively different regimes: (1) U_2/U_0=0, (2) $U_2/U_0>0$ (we use U_2/U_0=0.03 since this is appropriate for ^{23}Na, and (3) $U_2/U_0<0$ as in ^{87}Rb (for specificity, we use U_2/U_0=−0.03).

We first consider U_2/U_0=0, which can be achieved when the scattering lengths are equal, i.e., $a_0=a_2$. In this case, the on-site interaction between bosons is spin independent. This leads to an infinitely degenerate superfluid state: Specifically, for a given value of the superfluid density ρ_s, the three order parameters $\psi_\sigma, \sigma=-1$, 0, and 1, can have any magnitudes that satisfy Eq. (9); e.g., if we make the specific choice $\psi_{-1}=\psi_1$, then the pseudograyscale plot of Fig. 1(b) shows that the minima of the variational mean-field energy at T=0 lie on the ellipse $2\psi_1^2+\psi_0^2=\rho_s$. This degeneracy makes the superfluid phase of the spin-1 Bose-Hubbard model different from its spin-0 counterpart *even if* U_2=0, and it implies that an infinite number of SF phases *coexist* at U_2=0. However, the zero-temperature phase diagram of Fig. 1(a) is the same as that of spinless Bose-Hubbard model;[5] and, in particular, lobes of the MI phase are separated from the SF phase by the SF-MI boundaries that are all continuous at T=0; the density ρ is fixed at integral values in each MI lobe.

Striking differences between the spin-1 and spinless cases appear at finite temperatures. We demonstrate this in Figs. 1(a) and 2; the former compares phase diagrams at T=0 and T=0.05, and the latter presents plots, both at T=0 and T=0.05, of the superfluid density ρ_s and the density ρ as functions of the chemical potential μ for three different values of the on-site interaction U_0 (=4, 5, and 6). [In both spinless and spin-1 cases, if U_2=0, the tip of the first lobe lies at $U_{0C}(\rho=1)\simeq 5.8$ for T=0.[5,13]] Figure 1(a) shows that $U_{0C}(\rho)$ decreases as the T increases, i.e., the MI lobes grow at the expense of the SF phase. Figure 2 shows that ρ_s goes to zero continuously at the SF-MI transition if T=0, but with a jump if T=0.05. Thus, the SF-MI transition becomes a first-order transition at finite T and the zero-temperature SF-MI boundaries [Fig. 1(a)]are really lines of tricritical points; as the temperature is increased further, the first-order transition again becomes continuous at another tricritical point.

The first-order, SF-MI coexistence boundary is associated with the three-degenerate-minima structure in the variational free-energy plots, shown in Fig. 3. To obtain these plots we

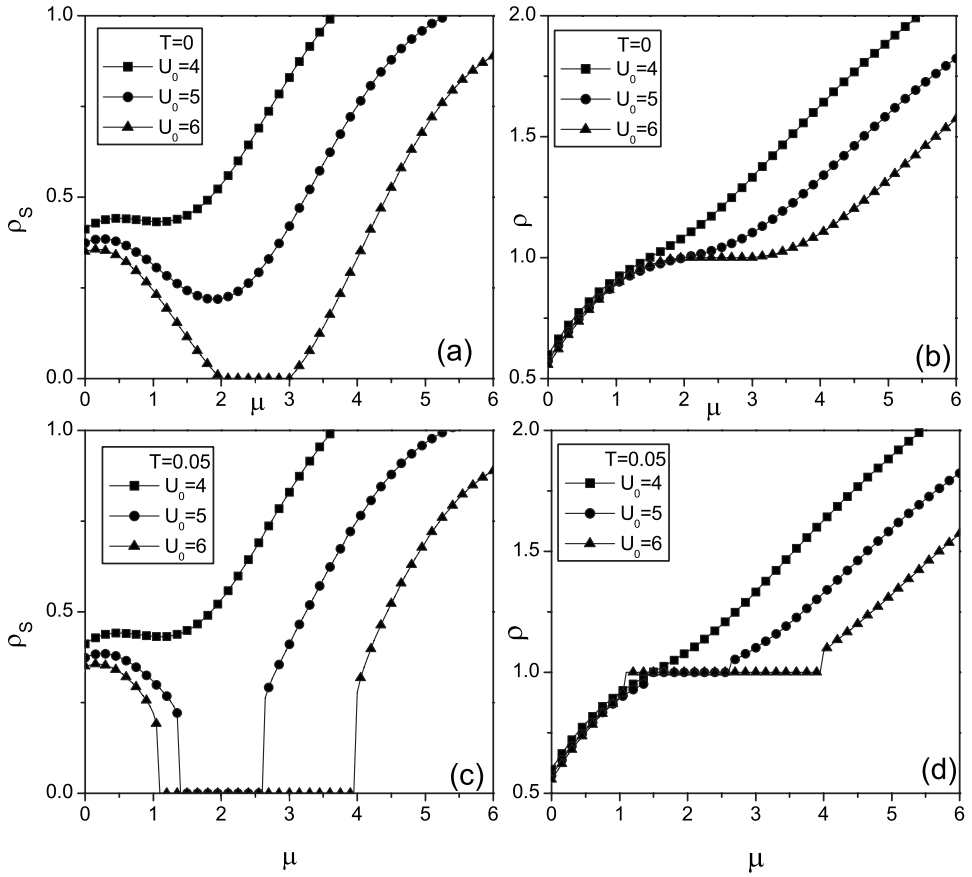

FIG. 2. Representative plots of (a) ρ_s and (b) ρ versus μ for $U_0=4$, 5, and 6, and $U_2=0$ at $T=0$. Similar plots at $T=0.05$ are given in (c) and (d). In the MI phases, $\rho_s=0$ and ρ is an integer [=1 in (b) for $U_0=6$] for $T=0$; for $0\lesssim T$, the MI phase evolves without a singularity (see text) into the NBL, in which ρ is exponentially close to an integer [=1 in (d) for $U_0=5$ and 6]. As the temperature increases from zero, the MI phases grow at the expense of SF phase and the SF-MI transition becomes of first order (see Fig. 1.

use $\psi_{-1}=\psi_0=\psi_1\equiv\psi$, which is one of the admissible solutions in the infinitely degenerate SF phase for the case $U_2=0$; the infinite degeneracy of this phase, illustrated for $T=0$ in Fig. 1(b), persists in our mean-field theory even if $T>0$. Figure 3 shows plots of the variational free energy $\mathcal{F}$ (ground-state energy $\mathcal{E}_0$ for $T=0$) as a function of ψ for different values of μ in the vicinity of the SF-MI transition; the minima at $\psi=0$ and $\psi\neq 0$ correspond, respectively, to MI and SF phases. At $T=0$, the SF-MI transition is continuous: this is reflected in the plots of $\mathcal{E}_0$ in Fig. 3(a), where, as we go from the SF to the MI phase by changing μ, two global minima with $\psi\neq 0$ merge to yield one minimum at $\psi=0$; precisely at the mean-field critical point, we have a *quartic* minimum. For $0\lesssim T$, $\mathcal{F}$ develops three degenerate minima at the SF-MI boundary, indicating clearly the coexistence of SF and MI phases at a first-order boundary. This boundary can be crossed either by changing μ at fixed T [Fig. 3(b)] or by changing T at fixed μ [Fig. 3(c)]. At sufficiently high temperatures, this three-minima structure of $\mathcal{F}$ goes away at a tricritical point at which the three minima coalesce to yield a *sixth-order* minimum. Beyond this tricritical point, the SF-MI transition is continuous (second order).

Calculations such as those summarized in the plots of Fig. 3 help us to obtain the phase diagrams shown in Figs. 4(a)–4(d) for $U_0=12$ and $U_2=0$. Let us begin with the μ-T phase diagram shown in Fig. 4(a). The MI phases [lobes in Fig. 1(a)] at $T=0$ evolve without any singularity into the NBL for $T>0$. As we have emphasized earlier, MI and NBL phases are not distinct, but it is useful to think of a smooth crossover from one to the other; we define these crossover boundaries as the loci of points at which the compressibility $\kappa_X=0.02$. The MI-NBL crossover boundaries (lines with filled triangles) are also shown in Figs. 4(a) and 4(c). To show the dependence of this crossover boundaries on the crossover value of the compressibility, we have computed this line for slightly different crossover values ($\kappa_X=0.01$, 0.02, and 0.03). The dependence of this line on these values is given in Fig. 4(c); though the position of this line changes, its shape does not undergo a qualitative change.

Islands of the SF phase appear in the μ-T phase diagram; the first two of these are shown in Fig. 4(a), where one is marked SF and the other, near the origin, is shown magnified in Figs. 4(b) and 4(c). The only difference between Figs. 4(b) and 4(c) is that the latter shows the MI-NBL crossover boundary (line with triangles) and a line with stars, the locus of points in the SF phase at which the variational free energy $\mathcal{F}$ goes from a curve with three minima to one with two minima. This line meets the SF-MI boundary at a tricritical point labeled TCP1. Higher islands of the SF phase show analogous tricritical points labeled TCP2, TCP3, etc.; the

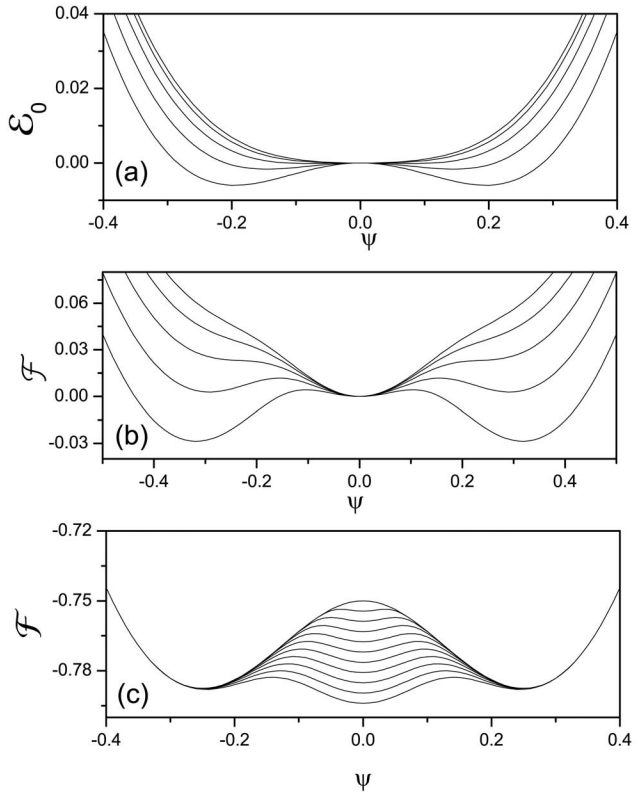

FIG. 3. Plots of the variational free energy $\mathcal{F}$ (ground-state energy $\mathcal{E}_0$ for $T=0$) as a function of ψ for different values of μ in the vicinity of the SF-MI transition for $U_2=0$ and with $\psi_{-1}=\psi_0=\psi_1 \equiv \psi$ (see text). The minima at $\psi=0$ and $\psi\neq 0$ correspond, respectively, to MI and SF phases. (a) The two minima at $\psi\neq 0$ merge into one minimum at $\psi=0$ to yield the mean-field continuous SF-MI transition at $T=0$ as we increase μ from 1.5 (bottom curve) to 2.3 (top curve) in steps of 0.2. Similar plots of $\mathcal{F}$ are given in (b) and (c). For $0\lesssim T$, $\mathcal{F}$ develops three degenerate minima at the SF-MI boundary, indicating clearly the coexistence of SF and MI phases at a first-order boundary. This boundary can be crossed either (b) by changing μ [from 0.7 (bottommost curve) to 1.5 (topmost curve) in steps of 0.2] at fixed $T=0.05$ or (c) by changing T [0 (topmost curve) to 0.1 (bottommost curve) in steps of 0.01] at fixed $\mu=2$.

SF-MI phase boundaries meet the $T=0$ axis at the zero-temperature tricritical points TCP01, TCP02, TCP03, etc. [Fig. 4(a)]. Figure 4(d) shows the density-temperature (ρ-T) version of part of the μ-T phase diagram of Fig. 4(a) (without the MI-NBL crossover line). The first-order parts of the SF-MI boundaries now appear as regions of two-phase coexistence that are hatched with tie lines. The two-phase regions corresponding to the two lowermost SF-MI boundaries in Fig. 4(a) are depicted; they end at the tricritical points TCP1 and TCP2, out of which emerge the continuous (second order) SF-MI phase boundaries. We use the label MI/NBL since there is no strict distinction between MI and NBL phases for $T>0$. Note that, in such a ρ-T phase diagram, the MI/NBL phases get pinched into exponentially small regions [e.g., in the vicinity of $\rho=1$ in Fig. 4(d)] as $T\to 0$ and two zero-temperature tricritical points get mapped onto each other [e.g., TCP01 and TCP02 in Fig. 4(d)].

We now investigate the case $U_2\neq 0$, so the on-site interaction between bosons depends on the spin. This lifts some of the infinite degeneracy we encountered in the case $U_2=0$ as can be seen directly at $T=0$ by comparing the pseudogray-scale plots of $\mathcal{E}_0$ in Figs. 1(b)–1(d), for $U_2=0$, $U_2>0$, and $U_2<0$, respectively.

If $U_2<0$, there are four degenerate minima, each corresponding to a ferromagnetic SF, with $\psi_{-1}=\psi_1$ and $\psi_0=\pm\sqrt{2}\psi_{\pm 1}$. The zero-temperature, mean-field, phase diagram for this case is shown in Fig. 5; it has the same topology as the phase diagram for the case $U_2=0$ [Fig. 1(a)]. We see that the MI phases have shrunk marginally and the SF-MI transitions are still continuous. The continuous nature of the $T=0$, SF-MI transition is illustrated by the continuous variation of $\psi_{\pm 1}$, ψ_0, and ρ_s as functions of μ in Fig. 6. The parameter $\langle\vec{F}\rangle^2$, defined only in the SF phase, assumes the value 1, which confirms that we have a ferromagnetic SF phase in this case. The μ-T phase diagram for the case $U_2<0$ has the same topology as the $U_2=0$ phase diagrams of Fig. 4. We do not show the μ-T phase diagram for $U_2<0$ since, for the parameters we use, namely, $U_0=12$ and $U_2/U_0=-0.03$, the phase boundaries are very close to those in Fig. 4.

If $U_2>0$, there are four degenerate minima of the variational free energy $\mathcal{F}$ shown, e.g., at $T=0$ in the pseudogray-scale plot of Fig. 1. Each one of these minima corresponds to a polar SF, with either $\psi_{-1}=\psi_1\neq 0$ and $\psi_0=0$ or vice versa, as shown in the plots of $\psi_{\pm 1}$ and ψ_0, versus μ in Fig. 7 for $U_2/U_0=0.03$. The parameter $\langle\vec{F}\rangle$, defined only in the SF phase, assumes the value 0, which also confirms that we have a polar SF phase. The zero-temperature, mean-field, phase diagram for this case is shown in Fig. 8. If the density ρ is equal to an odd integer ($\rho=1$ is shown in Fig. 8), this phase diagram has the same form as its counterpart for $U_2=0$ [Fig. 1(a)]. We see that the MI lobes expand marginally, and the SF-MI transitions are still continuous. However, if the density ρ is equal to an even number ($\rho=2$ is shown in Fig. 8), the SF-MI transition becomes of first order and the MI phase is stable over a much wider region of parameter space than for the case $U_2=0$: As we show in Fig. 9, for $U_2/U_0=0.03$, $U_0=7$, and $T=0$, ρ_s and ρ vary continuously as functions of μ at the SF-MI transition for $\rho=1$ but discontinuously for $\rho=2$. For comparison, we also include the plots for $U_2=0$. (We use $U_0=7$ here, rather than $U_0=12$, to compress the range of μ over which the SF-MI transitions occur.)

For $\rho=2$ in the MI phase, there are exactly two bosons localized per site and the total spin at every site can be either $S=0$ or $S=2$. Since $U_2>0$, there is an energy difference between the $S=0$ and $S=2$ states, with a lower energy for the singlet state. To go from the MI to the SF phase, this singlet state has to be broken by supplying an energy $\sim U_2$, which gives a rough estimate for the *latent heat* of this first-order transition if $0\lesssim T$. This requirement of a latent heat leads to the greater stability of the MI phases for even values of ρ relative to their counterparts for odd values of ρ. Thus, the $\rho=2$ MI lobe in Fig. 8 is substantially larger than the one for $\rho=1$. The μ-T phase diagram for the case $U_2>0$, shown in Fig. 10(a), for $U_0=12$ and $U_2/U_0=0.03$, has nearly the same form as the $U_2=0$ phase diagram of Fig. 4. The principal

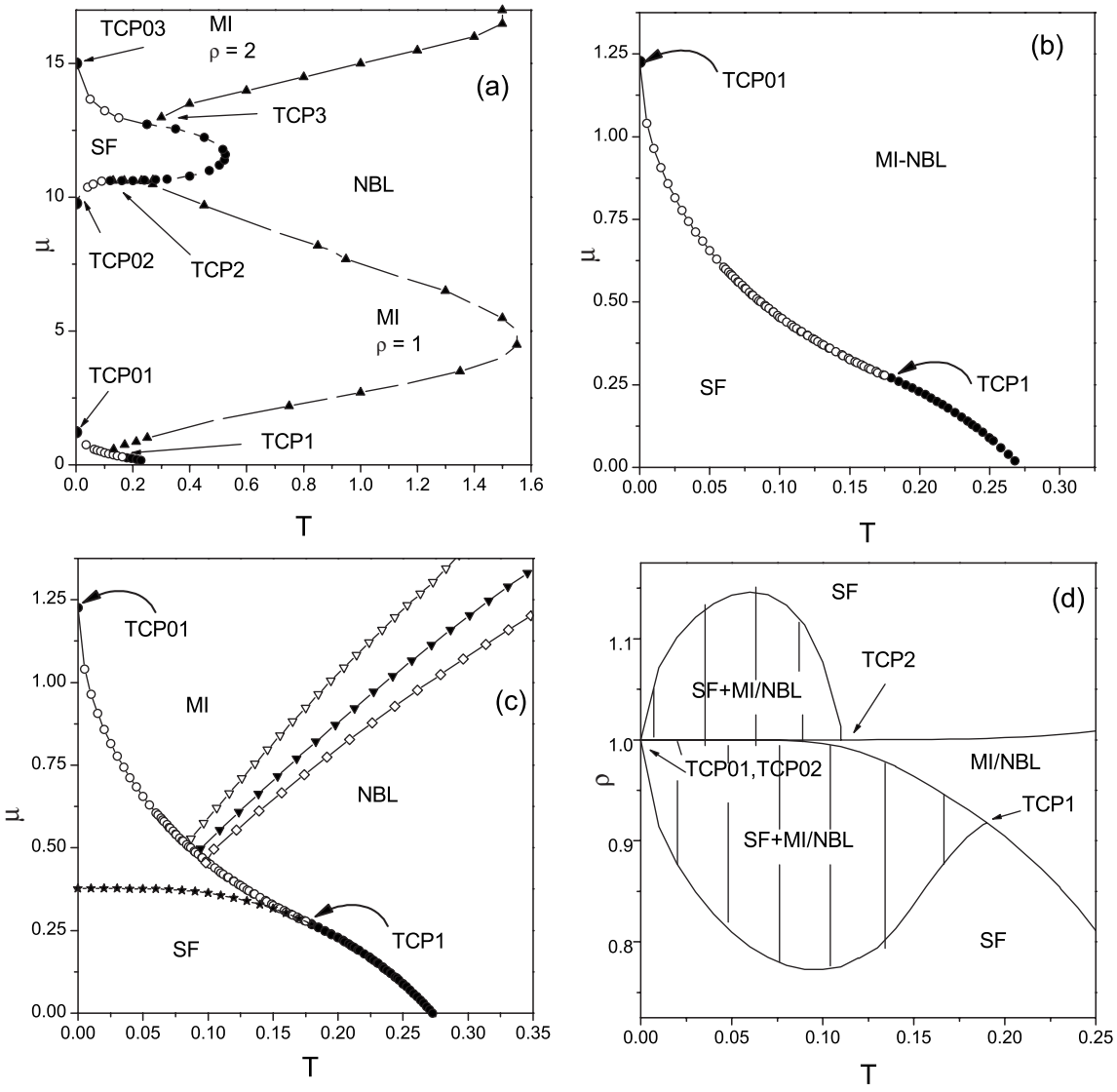

FIG. 4. (a) Mean-field phase diagram in the μ-T plane for $U_0=12$ and $U_2=0$. Lines with open (filled) circles represent first-order (continuous) SF-MI/NBL phase boundaries. First-order and continuous boundaries meet at tricritical points (TCPs). The $T=0$ ($T>0$) tricritical points are labeled TCP01, TCP02, etc. (TCP1, TCP2, etc.). The line with filled triangles represents the crossover boundary between MI and NBL regions of the MI/NBL phase. The lower left corner of the phase diagram in (a) is enlarged in (b) and (c). The only difference between (b) and (c) is that the latter shows the MI-NBL crossover boundary (lines with open, filled triangles, and open diamonds, respectively, for slightly different crossover values of $\kappa_X=0.01$, 0.02, and 0.03) and a line with stars, the locus of points in the SF phase at which the variational free energy $\mathcal{F}$ goes from a curve with three minima to one with two minima; this line meets the SF-MI boundary at TCP1. (d) The density-temperature (ρ-T) version of part of the μ-T phase diagram of (a) (without the MI-NBL crossover line); tie lines are used to hatch the two-phase regions in which SF and MI/NBL phases coexist (see text).

qualitative difference between these phase diagrams is that, if $U_2>0$, there are no zero-temperature, tricritical points for the first-order boundaries associated with the MI lobes for even values of ρ; e.g., the tricritical point TCP03 in Fig. 4 has no counterpart in Fig. 10(a). A quantitative comparison between these two phase diagrams is made in Fig. 10(b); this shows that the two phase diagrams are nearly indistinguishable except for the first-order boundaries that link the zero-temperature, SF-MI transitions for even values of ρ with the tricritical points directly above them (e.g., TCP3). In Fig. 10(b), the dashed line with open circles (open diamonds) is the first-order boundary for $U_2/U_0=0.03$ ($U_2=0$). The region **I** between these lines lies in the MI (SF) phase if $U_2/U_0=0.03$ ($U_2=0$). The lines with filled triangles show the MI-NBL crossover as in Fig. 4(a). Phase diagrams such as Fig. 10 are obtained by calculating the order parameters ψ_σ, and thence ρ and ρ_s, as functions of μ at different temperatures. Representative plots are shown in Fig. 11 for $U_2/U_0=0.3$ and $U_0=7$, and $T=0$ and $T=0.05$.

IV. CONCLUSIONS

We have carried out the most extensive study of the phase diagram of the spin-1 Bose-Hubbard model so far by gener-

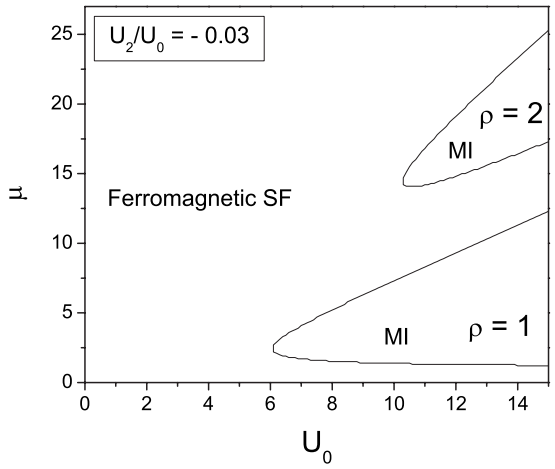

FIG. 5. Mean-field phase diagram in the (μ-U_0) plane for $U_2/U_0=-0.03$ and $T=0$. This has the same topology as the phase diagram for the case $U_2=0$ [Fig. 1(a) for $T=0$], but the MI lobes shrink marginally; the SF-MI transitions are continuous.

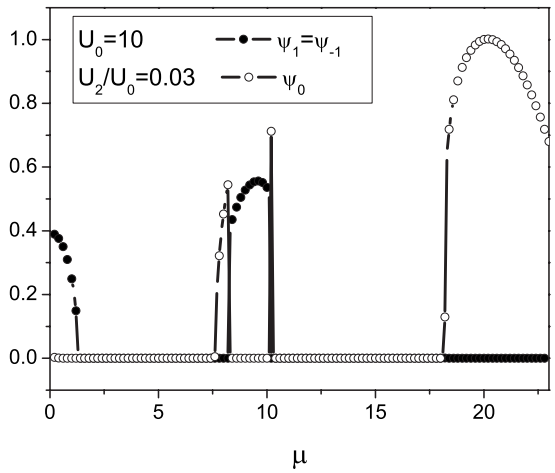

FIG. 7. Mean-field values of the superfluid order parameters $\psi_1=\psi_{-1}$ and ψ_0 plotted as functions of μ for $U_0=10$, $U_2/U_0=0.03$, and $T=0$. The SF phase has either $\psi_{-1}=\psi_1\neq 0$ and $\psi_0=0$ or vice versa, which confirms that we have a polar SF in this case.

alizing an intuitively appealing mean-field theory that has been used earlier for the spinless case. Our study yields both zero-temperature and finite-temperature phase diagrams for this model. Only $T=0$ phase diagrams had been obtained so far,[11–13] so our elucidation of the finite-temperature properties of this model yield qualitatively different insights. We find, in particular, that several of the SF-MI transitions in this model are generically of first order; at sufficiently high temperatures, they become continuous via tricritical points. Tricritical points also abound at zero temperature since some, but not all, of the finite-temperature first-order transitions become continuous as $T\rightarrow 0$. The resulting phase diagrams (Figs. 4 and 10) are very rich and should provide a challenge for experimental studies, which we hope our work will stimulate. Experiments can study both the case $U_2<0$, which can be realized possibly by using ^{87}Rb, and the case $U_2>0$, which can be realized by using ^{23}Na. Thus, in principle, both the phase diagrams of Figs. 4 and 10 could be obtained experimentally. Of course, this will require good experimental control of both the temperature and the density (or chemical potential) of the bosons.

Our mean-field theory has been shown[5,6] to yield good results for the spin-0 Bose-Hubbard model. In particular, mean-field-theory plots of the scaled superfluid density ρ_s/ρ versus the scaled interaction U/U_c lie close to each other; at worst, the disagreement is $\simeq 22\%$ in two-dimensional. Monte Carlo results. The mean-field-theory prediction for U_C

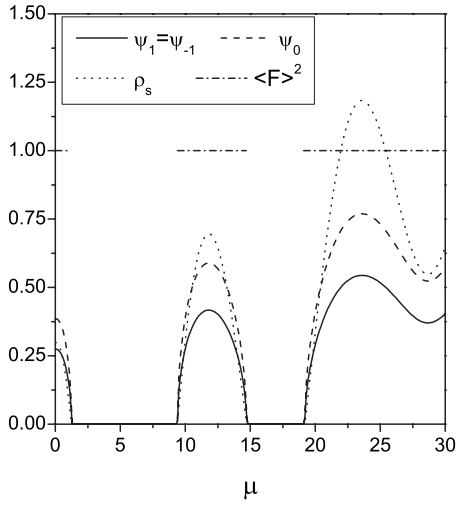

FIG. 6. Mean-field values of the superfluid order parameters $\psi_1=\psi_{-1}$ and ψ_0, and ρ_s plotted as functions of μ for $U_0=12$, $U_2/U_0=-0.03$, and $T=0$; ρ_s goes to zero continuously at the SF-MI transitions. The parameter $\langle\vec{F}\rangle^2$, defined only in the SF phase, assumes the value 1, which confirms that we have a ferromagnetic SF phase in this case.

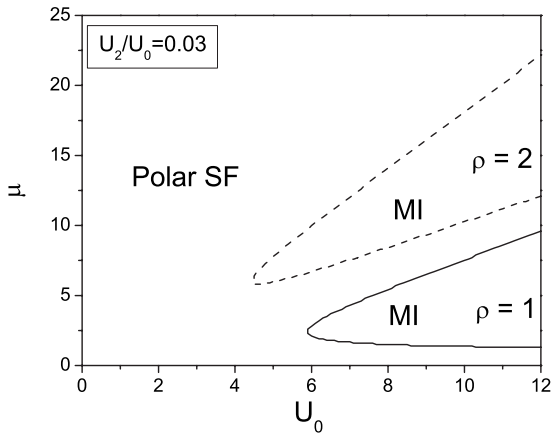

FIG. 8. Mean-field phase diagram in the (μ-U_0) plane for $U_2/U_0=0.03$ and $T=0$. The $\rho=1$ MI lobe has the same form as its counterpart for $U_2=0$ [Fig. 1(a)]. We see that the MI lobes expand marginally, and the SF-MI transitions are continuous (represented by a continuous line), but for $\rho=2$, the SF-MI transition becomes of first order (represented by a dashed line) and the MI phase is stable over a much wider region of parameter space than for the case $U_2=0$.

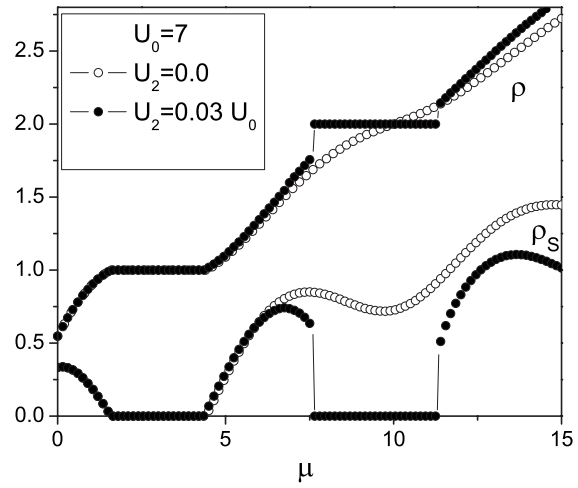

FIG. 9. Plots of ρ_s and ρ as function of μ for $T=0$, $U_0=7$, and $U_2/U_0=0.03$ (filled circles) and $U_2=0$ (open circles). In the former case, ρ_s changes continuously at the SF-MI transitions at the boundary of the $\rho=1$ MI lobe (Fig. 8), but jumps at the first-order SF-MI transitions associated with the boundary of the $\rho=2$ MI lobe. For $U_2=0$, only the $\rho=1$ lobe is encountered in this plot and the SF-MI transitions are continuous; ρ_s shows a gentle minimum in the vicinity of the $\rho=2$ MI lobe.

$\simeq 5.83z$, where the nearest-neighbor coordination number z is $2d$, for a d-dimensional hypercubic lattice. Recent Monte Carlo simulations yield $U_C \simeq 29.34$ (Ref. 16) for $d=3$, and $\simeq 16.74$ (Ref. 17) if $d=2$; these are, respectively, 19.14% and 39.31% lower than the mean-field-theory predictions. (Note, by contrast, that mean-field-theory predictions for the critical temperature in the three- and two-dimensional Ising models are too large by 32.98% and 76.27%, respectively.) Of course, mean-field-theory cannot hope to capture the nature of fluctuations in the superfluid and Mott-insulator phases. To the best of our knowledge, there are no Monte Carlo simulations for the spin-1 Bose-Hubbard model that yield its phase diagram and parameters such as U_C, so we cannot give a quantitative comparison of our mean-field-theory predictions for the spin-1 case with simulations. It is worth noting, however, that the MI-SF transitions in the spin-1 case can be of first order if $U_2>0$; here, mean-field theory should be especially good since there should be no diverging correlation length at this transition.

As we mentioned in Sec. I, our mean-field theory can be generalized to the case $V_T>0$. Such a generalized mean-field theory has to be inhmogeneous, i.e., the order parameters and, therefore, the single-site, mean-field Hamiltonian depend on the site label. For the formulation of such an inhomogeneous mean-field theory, for spin-0 bosons in a random chemical potential, see Ref. 6. We have carried out a detailed study of such an inhomogeneous mean-field theory for spin-1 bosons, $V_T>0$ and $T=0$; the variational energy now has to be minimized with respect to a very large number of site-dependent order parameters ($\simeq 40\,000$ for a 121^3 lattice in three dimensions). Such a calculation leads to alternating shells of superfluid and Mott-insulator shells in the optical lattice, as has been noted recently for the spin-0 case.[18,19] A full description of our inhomogeneous mean-field theory lies

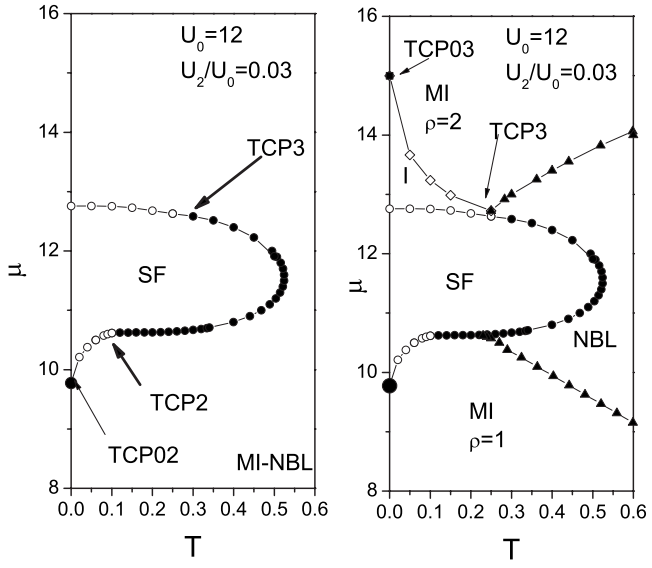

FIG. 10. (a) Mean-field phase diagram in the (μ-T) plane for $U_0=12$ and $U_2/U_0=0.03$ showing first-order (open circles) and continuous (filled circles) transitions between SF and MI/NBL phases and TCPs. This phase diagram is nearly the same as the $U_2=0$ phase diagram (Fig. 4), but there are no zero-temperature, tricritical points for the first-order boundaries associated with the MI lobes for even values of ρ: e.g., TCP03 in Fig. 4 has no counterpart here. (b) A quantitative comparison between these two phase diagrams shows that the two phase diagrams are nearly indistinguishable except for the first-order boundaries that link the zero-temperature, SF-MI transitions for even values of ρ with the tricritical points directly above them (TCP3 here); lines with open circles (open diamonds) denote the first-order boundaries for $U_2/U_0=0.03$ ($U_2=0$). The region **I** between these lines lies in the MI (SF) phase if $U_2/U_0=0.03$ ($U_2=0$). The lines with filled triangles show the MI-NBL crossover boundary.

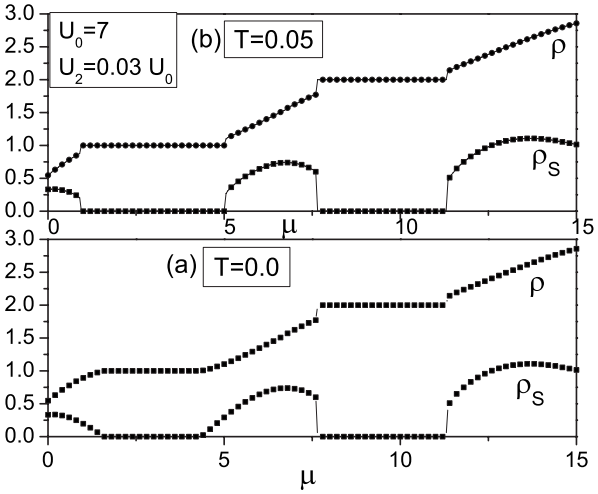

FIG. 11. Representative plots of ρ_s and ρ versus μ for (a) $T=0$ and (b) $T=0.05$ for $U_0=7$ and $U_2/U_0=0.03$ showing jumps at first-order SF-MI transitions; ρ_s changes continuously at the $T=0$, continuous SF-MI transition associated with the $\rho=1$ MI lobe.

well outside the scope of this paper and will be presented elsewhere.

Our mean-field theory has been designed to investigate the relative stabilities of SF and MI/NBL phases. It has predicted the even-odd asymmetry in the Mott-insulator lobes. This feature of the phase diagram has also been predicted in one dimension using density-matrix renormalization group calculation.[20] Our mean-field theory has enough structure to unravel the differences between polar and ferromagnetic superfluids. However, our mean-field theory does not account for order parameters that can distinguish between different spin orderings in the MI phase, e.g., spin-singlet and nematic MIs, which have been investigated in the limit $U_0 \to \infty$ by some groups.[21,22] The generalization of our mean-field theory to include such types of structures in the MI phases of model (1) lies beyond the scope of this study, but is an interesting challenge for further theoretical work.

ACKNOWLEDGMENTS

One of us (R.V.P.) thanks the Jawaharlal Nehru Centre for Advanced Scientific Research and the Department of Physics, Indian Institute of Science, Bangalore for hospitality during the time when a part of this paper was written. This work was supported by DST, India (Grants No. SP/S2/M-60/98 and No. SP/12/PF-01/2000) and UGC, India.

*rvpai@unigoa.ac.in
†kshesh@gmail.com
‡Also at Jawaharlal Nehru Centre for Advanced Scientific Research, Jakkur, Bangalore 560 064, India; rahul@physics.iisc.ernet.in; URL: http://www.physics.iisc.ernet.in/~rahul

[1] F. Dalfovo, S. Giorgini, L. P. Pitaevskii, and S. Stringari, Rev. Mod. Phys. **71**, 463 (1999); I. Bloch, J. Dalibard, and W. Zwerger, arXiv:0704.3011bv1 [cond-mat.other] Rev. Mod. Phys. (to be published); M. Lewenstein, A. Sanpera, V. Ahufinger, B. Damski, A. Sen, and U. Sen, Adv. Phys. **56**, 243 (2007).
[2] Subir Sachdev, *Quantum Phase Transitions* (Cambridge University Press, Cambridge, England, 1999).
[3] M. Greiner, O. Mandel, T. Esslinger, T. W. Hänsch, and L. Bloch, Nature (London) **415**, 39 (2002).
[4] D. Jaksch, C. Bruder, J. I. Cirac, C. W. Gardiner, and P. Zoller, Phys. Rev. Lett. **81**, 3108 (1998).
[5] K. Sheshadri, H. R. Krishnamurthy, R. Pandit, and T. V. Ramakrishnan, Europhys. Lett. **22**, 257 (1993).
[6] K. Sheshadri, H. R. Krishnamurthy, R. Pandit, and T. V. Ramakrishnan, Phys. Rev. Lett. **75**, 4075 (1995).
[7] D. M. Stamper-Kurn, M. R. Andrews, A. P. Chikkatur, S. Inouye, H. J. Miesner, J. Stenger, and W. Ketterle, Phys. Rev. Lett. **80**, 2027 (1998).
[8] T. L. Ho, Phys. Rev. Lett. **81**, 742 (1998).
[9] T. Ohmi and K. Machida, J. Phys. Soc. Jpn. **67**, 1822 (1998).
[10] S. Mukerjee, C. Xu, and J. E. Moore, Phys. Rev. Lett. **97**, 120406 (2006).
[11] T. Kimura, S. Tsuchiya, and S. Kurihara, Phys. Rev. Lett. **94**, 110403 (2005).
[12] K. V. Krutitsky and R. Graham, Phys. Rev. A **70**, 063610 (2004); K. V. Krutitsky, M. Timmer, and R. Graham, Phys. Rev. A **71**, 033623 (2005).
[13] R. V. Pai, K. Sheshadri, and R. Pandit, in *Current Topics in Atomic, Molecular, and Optical Physics*, edited by C. Sinha and S. Bhattacharyya (World Scientific, Singapore, 2007), pp. 105–119.
[14] C. K. Law, H. Pu, and N. P. Bigelow, Phys. Rev. Lett. **81**, 5257 (1998).
[15] We have checked that this value of n_{max} suffices for the large values of U_0 we use by comparing our results with those for $n_{max}=2$ and 3.
[16] B. Capogrosso-Sansone, N. V. Prokofev, and B. V. Svistunov, Phys. Rev. B **75**, 134302 (2007).
[17] B. Capogrosso-Sansone, S. G. Söyler, N. V. Prokofev, and B. V. Svistunov, arXiv:cond-mat/0710.2703v3 (unpublished).
[18] S. Wessel, F. Alet, M. Troyer, and G. G. Batrouni, Phys. Rev. A **70**, 053615 (2004).
[19] S. Fölling, A. Widera, T. Muller, F. Gerbier, and I. Bloch, Phys. Rev. Lett. **97**, 060403 (2006).
[20] M. Rizzi, D. Rossini, G. De Chlara, S. Montangero, and R. Fazio, Phys. Rev. Lett. **95**, 240404 (2005).
[21] J. Arlt, K. Dholakia, J. Soneson, and E. M. Wright, Phys. Rev. A **63**, 063602 (2001).
[22] G. Fáth and J. Sólyom, Phys. Rev. B **51**, 3620 (1995).